

Spectroscopy of capacitively coupled Josephson-junction qubits

Philip R. Johnson, Frederick W. Strauch, Alex J. Dragt, Roberto C. Ramos, C. J. Lobb, J.R. Anderson, and F. C. Wellstood

Department of Physics, University of Maryland, College Park, MD 20742-4111
(Dated: February 7, 2020)

We develop the theory of two capacitively-coupled Josephson junctions in the quantum limit, and show that the junctions form a simple coupled qubit system with effective coupling controlled by the junction bias currents. Given the junction parameters and coupling capacitance, we compute numerically the energy levels and wavefunctions for the system. The dependence of the energy levels on the parameters can be measured spectroscopically, providing an important experimental test for the presence of entangled multi-qubit states in Josephson junction based circuits.

PACS numbers: 74.50.+r, 03.67.Lx, 85.25.Cp

Keywords: Qubit, quantum computing, superconductivity, Josephson junction.

Ramos *et al.* have proposed that electrically well-isolated Josephson junctions can be used as qubits [1]. Two recent experiments using different isolation schemes have reported Rabi oscillations in single junctions [2], demonstrating the existence of macroscopic quantum coherence. While longer coherence times are desirable, these experiments show that single Josephson junctions are strong candidates for solid-state qubits; several different superconducting Josephson based types have been proposed [3].

One of the next major steps towards building a Josephson junction based quantum computer will be the observation of quantum properties of coupled macroscopic qubits. A simple scheme for making coupled qubits, junctions connected by capacitors, has recently been proposed by Blais *et al.* [4] and Ramos *et al.* [5]. This scheme is illustrated for the two-qubit case in Fig. 1 (a).

In this paper we calculate, using highly accurate numerical methods, the energy levels and metastable wavefunctions for the circuit of Fig. 1 (a) in terms of the junction parameters, bias currents, and coupling capac-

itance. Our numerical analysis demonstrates that the system can be tuned sufficiently to create appropriately spaced energy levels and coupled states. The features that we discuss can both guide the experimental effort of observing multi-qubit quantum states and provide help in optimizing the design of qubits and gates. Experimental observation of these macroscopic entangled quantum states will be an important achievement in its own right, and will provide strong support for the validity of macroscopic quantum mechanics and the existence of macroscopic entanglement [6].

The Hamiltonian for an ideal single current-biased Josephson junction, with critical current I_c and junction capacitance C_J , is

$$H(\gamma, p) = (4E_C\hbar^{-2})p^2 - E_J(\cos\gamma + J\gamma), \quad (1)$$

where γ is the gauge-invariant phase difference across the junction, $J = I/I_c$, I is the (tunable) bias current, $E_J = (\Phi_0 I_c/2\pi)$ is the Josephson energy, $E_C = e^2/2C_J$ is the charging energy, and $\Phi_0 = h/2e$ is the flux quantum. The canonical momentum is $p = (\Phi_0/2\pi)^2 C_J \dot{\gamma} = \hbar Q/2e$, where Q is the charge on the junction. The ratio of the Josephson energy to the charging energy, E_J/E_C , determines whether the system is in a phase, charge, or intermediate regime. The qubits explored in this paper have $E_J \gg E_C$ and hence are in the phase regime.

The equations of motion for a single current-biased junction are equivalent to the motion of a particle in the tilted washboard potential shown in Fig. 1 (b). Classically, for $J < 1$ there are stable minima about which the phase can oscillate with the characteristic plasma frequency $\omega_p(J) = \sqrt{2\pi I_c/\Phi_0 C_J} (1 - J^2)^{1/4}$. Quantum mechanically, the system exhibits localized metastable states in each well that can tunnel out into the running (finite-voltage) state. The effective barrier height $\Delta U_{\text{barrier}}$ (see Fig. 1 (b)) for a single junction in units of

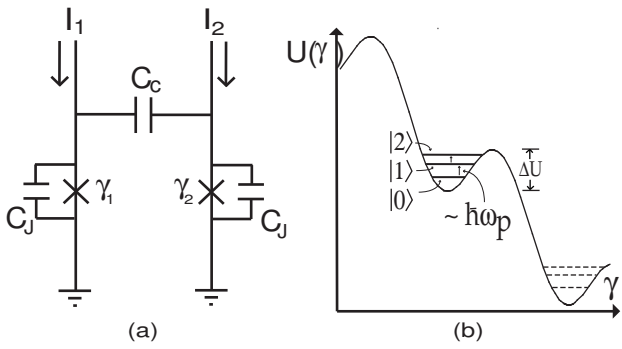


FIG. 1: (a) (left) Circuit diagram for two idealized capacitively coupled Josephson junctions. Fig. (b) (right) The tilted washboard potential for a single current-biased Josephson junction with three metastable quantum states.

$\hbar\omega_p(J)$ is

$$N_s \simeq \frac{\Delta U_{\text{barrier}}}{\hbar\omega_p(J)} = \frac{2^{3/4}}{3} \left(\frac{E_J}{E_C} \right)^{1/2} (1 - J)^{5/4}; \quad (2)$$

where N_s is the approximate number of metastable bound states for a single isolated junction. Our analysis explores effects when N_s is small, in which case the non-linearity of the potential is important. The metastable energy levels have been directly observed in resonant activation experiments [7].

By adjusting the bias current it is possible to tune the barrier height to obtain, for example, three metastable energy levels $E_0 < E_1 < E_2$ with the two lowest states forming the basis $|0\rangle, |1\rangle$ of a qubit. State $|2\rangle$ has the highest escape rate due to tunneling and can therefore act as an auxiliary readout state, where readout is achieved by microwave pumping at a frequency $\omega_{12} = (E_2 - E_1)/\hbar$. Detection of a voltage across the junction implies that the system was previously in the state $|1\rangle$ and has entered the running state.

The Hamiltonian for the coupled two-junction circuit shown in Fig. 1 (a) is:

$$H = \frac{4E_C}{(1 + \zeta)\hbar^2} (p_1^2 + p_2^2 + 2\zeta p_1 p_2) - E_J (\cos \gamma_1 - \cos \gamma_2 - J_1 \gamma_1 - J_2 \gamma_2), \quad (3)$$

where $\zeta = C_C/(C_C + C_J)$ is the dimensionless coupling parameter, C_C is the coupling capacitance, and $J_{1,2}$ are the normalized bias currents of junctions 1 and 2, respectively. The canonical momenta

$$p_{1,2} = (C_C + C_J) \left(\frac{\Phi_0}{2\pi} \right)^2 (\dot{\gamma}_{1,2} - \zeta \dot{\gamma}_{2,1}) = \left(\frac{\Phi_0}{2\pi} \right) (Q_{1,2} \pm Q_c) \quad (4)$$

are proportional to the charges $Q_{1,2}$ on each junction plus (or minus) the charge on the coupling capacitor plate adjacent to it [4, 5]. In Eq. (4) we adopt the convention, also used below in Eq. (7), where the subscript 1 is associated with the + sign and the subscript 2 is associated with the - sign.

Because momentum coupling is intuitively unfamiliar, we make a canonical change of variables that diagonalizes the kinetic energy part of the Hamiltonian:

$$H(p_+, p_-, \gamma_+, \gamma_-) = \frac{4E_C}{(1 + \zeta)\hbar^2} (p_+^2 + p_-^2) + V(\gamma_+, \gamma_-), \quad (5)$$

where

$$V(\gamma_+, \gamma_-) = -E_J (\cos \gamma_1 + \cos \gamma_2 + J_1 \gamma_1 + J_2 \gamma_2) \quad (6)$$

and

$$\gamma_{1,2} = \left(\gamma_+ \sqrt{1 + \zeta} \pm \gamma_- \sqrt{1 - \zeta} \right) / \sqrt{2}, \quad (7)$$

$$p_{\pm} = (p_1 \pm p_2) / \sqrt{2(1 \pm \zeta)}. \quad (8)$$

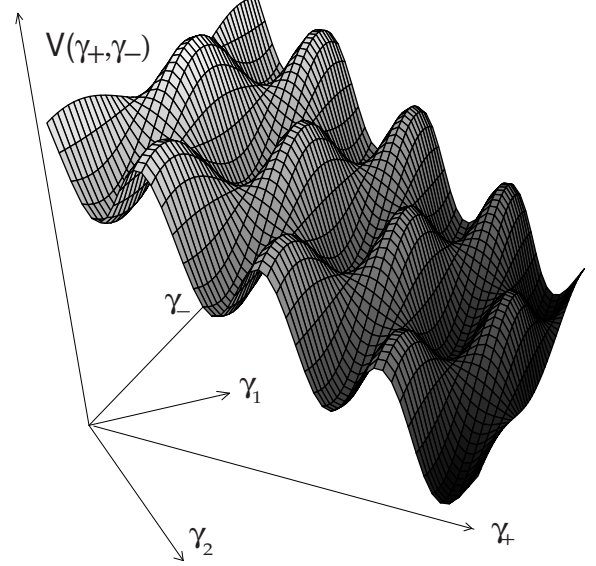


FIG. 2: Potential $V(\gamma_+, \gamma_-)$ for Hamiltonian in diagonal kinetic energy form.

The potential energy V for the strong coupling case $\zeta = 0.4$ with $J_1 = J_2 = 0.5$ is shown in Fig. 2. In the γ_{\pm} coordinates the coupling can be seen as an effective ‘squeezing’ along the γ_+ direction.

We can gain further insight into the coupling of the junction states by looking at the normal mode behavior for small oscillations, neglecting nonlinearities. For small coupling and detuned bias currents (J_1 far from J_2) the normal modes are approximately γ_1 and γ_2 , i.e., the junctions are effectively decoupled. When $J_1 = J_2$ the normal modes become γ_+ and γ_- , and we therefore expect the coupled junction states to be entangled symmetric and antisymmetric combinations of the single junction states.

The challenging demands of quantum computing require an accurate and precise quantitative description of the states going beyond simple perturbation theory. To achieve this, we have computed the states and energy levels numerically, for a subset of system parameters, using a split operator spectral method [8] applied to the full nonlinear washboard potential. Using these results we have confirmed that the much faster complex scaling method [9] applied to the cubic approximation of the full potential [6] is quite accurate. The fast complex scaling method then allows us to compute energy levels for a wide range of system parameters relevant to building qubits. A further important property of both of these numerical methods is that they are well-suited to finding metastable states in potentials that allow tunneling. The computed quantum states have been further tested by time-evolving them in the full nonlinear washboard potential using real time split operator methods, confirming that these states are quasi-stationary with tunneling rates consistent with

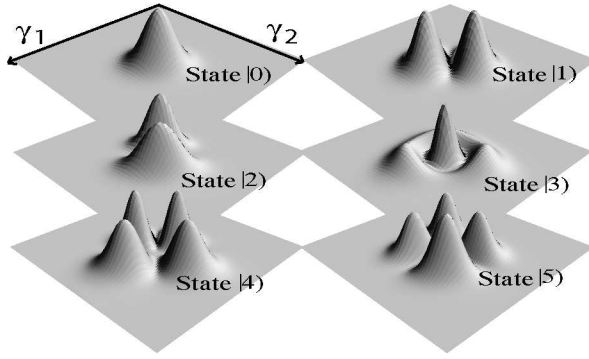


FIG. 3: The absolute value squared of the probability amplitude of the first 6 quasistationary wavefunctions for capacitively coupled current-biased Josephson junctions with coupling of $\zeta = 0.01$ and normalized bias currents of $J_1 = J_2 = 0.98693$.

higher-order WKB analysis.

In Fig. 3 we show, as an example, the numerically computed wavefunctions for identical junctions with capacitances $C_J = 4.3$ pF and critical currents $I_c = 13.3$ μ A. Junctions with these physical characteristics are readily fabricated and of physical interest. Figure 3 shows the squared absolute value of the wavefunction of the first 6 quasi-stationary states for the coupling strength $\zeta = 0.01$, and with the bias currents $J_1 = J_2 = 0.98693$. Isolated junctions would have approximately three quasi-stationary states ($N_s \simeq 3$). At such large bias currents the nonlinearities of the potential are pronounced, and the states deviate significantly from coupled harmonic oscillator states. The states $|n\rangle$ in Fig. 3 are ordered by energy E_n ; a rounded bracket has been used to distinguish the coupled two-junction states $|n\rangle$ from single junction states $|n\rangle$. The second and third states expressed in terms of single junction direct product states are $|1\rangle \cong (|01\rangle - |10\rangle)/\sqrt{2}$ and $|2\rangle \cong (|01\rangle + |10\rangle)/\sqrt{2}$, whereas the higher energy states are more complicated superpositions that depend upon the bias currents and coupling. The ordering of the states in Fig. 3 may be understood by looking at the potential shown in Fig. 2; wavefunctions that are extended in the γ_+ direction have higher energy because of the coupling induced effective squeezing in the γ_+ direction, relative to the γ_- direction.

For designing qubits out of coupled junctions we need to know how the energy levels depend on coupling and bias current. Figure 4 shows the effects of varying the coupling strength in the range $0 < \zeta < 0.2$ on the first 6 energy levels with $J_1 = J_2 = 0.98693$. The plasma frequency of each single junction when decoupled ($\zeta = 0$) is $\omega_p(J_1)/2\pi = \omega_p(J_2)/2\pi = 6.2037$ GHz. The bias currents have been chosen to enhance the nonlinearity. We have labeled the states at the left of Fig. 4 for zero coupling, where the product representation $|nm\rangle = |n\rangle \otimes |m\rangle$ is appropriate. Note that for zero coupling the nonlinear-

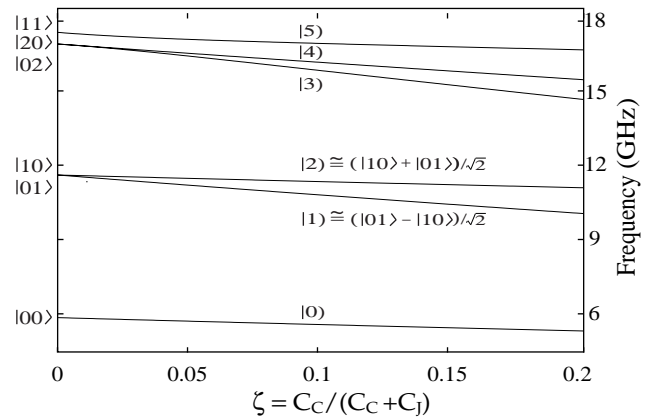


FIG. 4: Frequencies versus coupling strength for equal bias currents $J_1 = J_2 = 0.98693$, $I_C = 13.3$ μ A, and $C_J = 4.3$ pF. The states are labeled as single junctions product states at the far left where $\zeta = 0$.

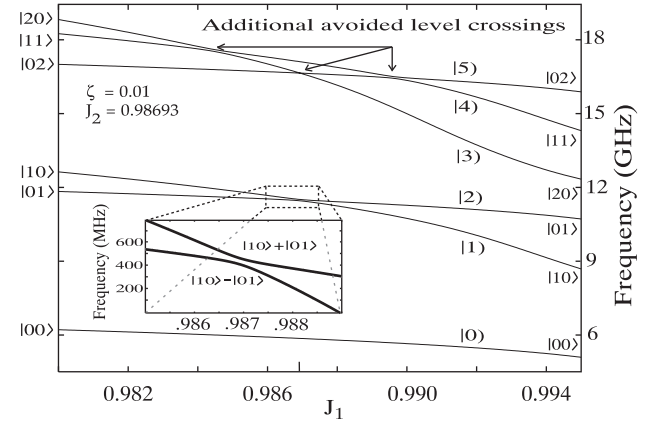


FIG. 5: Frequencies of the first 6 states versus bias current J_1 with $J_2 = 0.98693$ fixed and a coupling strength of $\zeta = 0.01$, $I_C = 13.3$ μ A, and $C_J = 4.3$ pF. The states are effectively decoupled at the far left and right where they are close to being single junction product states.

ity of the potential has broken the degeneracy between $|5\rangle = |11\rangle$ and the pair $(|3\rangle = |02\rangle, |4\rangle = |20\rangle)$, which remain degenerate when $\zeta = 0$.

In real experiments, the coupling strength ζ will typically be fixed by the circuit design, and can only be varied by making a completely new sample. By contrast, the bias currents through each junction are easily varied, and provide an efficient experimental probe of the entangled states shown in Fig. 3. Figure 5 shows how the energy levels change for $\zeta = 0.01$ and $J_2 = 0.98693$ fixed, while J_1 is varied around J_2 . There are promi-

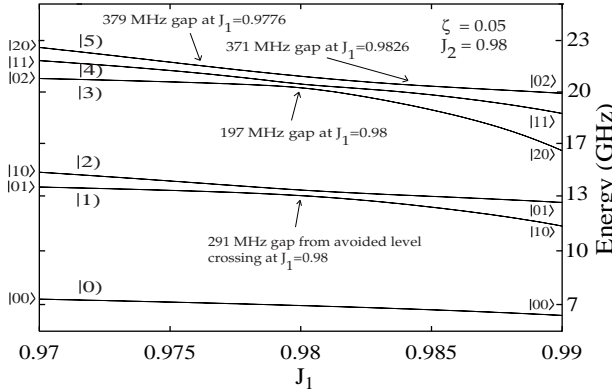


FIG. 6: Frequencies versus bias current J_1 with $J_2 = 0.98$ fixed and a coupling strength of $\zeta = 0.05$, $I_C = 13.3 \mu\text{A}$, and $C_J = 4.3 \text{ pF}$.

uent avoided level crossings indicated in the figure both on-tune ($J_1 = J_2$) and off-tune ($J_1 \neq J_2$). The predicted gap for the $|1\rangle, |2\rangle$ on-tune splitting at $J_1 = 0.98693$ is 57 MHz for $I_C = 13.3 \mu\text{A}$ and $C_J = 4.3 \text{ pF}$. The predicted gap for the first off-tune splitting between states $|4\rangle$ and $|5\rangle$ at $J_1 = 0.98444$ is 80 MHz, and for the second off-tune splitting at $J_2 = 0.99727$ the gap is 72 MHz. The predicted gap for the on-tune $|3\rangle, |4\rangle$ splitting of 4 MHz is much smaller than the others because it is a second order avoided crossing in perturbation theory. Figure 6 shows the energy levels for the same junction parameters as shown in Fig. 5 but with $\zeta = 0.05$ and $J_2 = .98 (N_s \simeq 5)$.

We have labeled the states in Figs. 5 and 6 at the far left and right—when the currents are detuned and hence the states are effectively uncoupled—as product states. This labeling is only strictly correct when $\zeta = 0$. The mixing that occurs between states when the bias currents are brought into tune is indicated for the states $|1\rangle$ and $|2\rangle$ in Figs. 4–6.

Experimental data similar to Figs. 5 and 6 would be important first evidence for the existence of macroscopic entangled states like those shown in Fig. 3. The energy levels of these entangled states should be readily observable using current experimental techniques. A typical experiment to probe the energy levels in Figs. 4-6 would proceed by preparing the system in the ground state $|0\rangle$ by cooling well below $T \simeq \omega_{01}\hbar/k \simeq 300$ mK. Varying the bias current J_1 while simultaneously injecting microwaves at a frequency ω^* should lead to an enhancement in the tunneling from the zero-voltage state to the finite-voltage running state of the system when $\omega^* = \omega_{ij}(J_1)$. This enhancement produces a corresponding peak in escape rate measurements [7]. By varying ω^* and J_1 we may map out the energy levels for comparison with Figs. 5 and 6.

Experimentally, the expected energy gap between the

avoided levels can be resolved if both the quality factor Q and coupling ζ of the system are reasonably large. For example, with the typical junction parameters assumed here, and with $\zeta = 0.01$, the predicted gap for the $|1\rangle, |2\rangle$ splitting of 57 MHz can easily be resolved with a Q of 200 [5], though the second order splitting of the $|3\rangle$ and $|4\rangle$ levels will be more challenging to see. However, these splittings will be easier to detect with a larger coupling capacitance (see Fig. 6).

In conclusion, we have presented predictions for experiments that probe macroscopic entangled states by the relatively simple scheme of doing spectroscopy on coupled junctions while varying external bias currents. The numerical methods we have used are powerful tools for mapping out the metastable states of the nonlinear, many-level coupled qubit system, and allow us to explore a wide range of junction parameters and couplings. This kind of detailed study will be necessary for the design of realistic coupled qubits.

Acknowledgements: We would like to thank Andrew J. Berkley, Huizhong Xu, and Mark A. Gubrud for helpful discussions. This work was supported in part by the U.S. Department of Defense and the State of Maryland, through the Center for Superconductivity Research.

- [1] R. Ramos et al., IEEE Trans. On Appl. Supercond. **11**, **998** (2001).
- [2] Y. Yu et al., Science **296**, 889 (2002); J. M. Martinis et al., Phys. Rev. Lett. **89**, 117901 (2002); M. H. Devoret, J. M. Martinis, and J. Clarke, Phys. Rev. Lett. **55**, 1908 (1985).
- [3] S. Han, R. Rouse, and J. E. Lukens, Phys. Rev. Lett. **76**, 3404 (1996); M. F. Bocko, A. M. Herr, and M. J. Feldman, IEEE Trans. Appl. Supercon. **7**, 3638 (1997); J. E. Mooij et al., Science **285**, 1036 (1999); C. H. van der Wal et al., Science **290**, 773 (2000); J.R. Friedman et al., Nature (London) **406**, 43 (2000); Y. Makhlin, G. Schön, and A. Shnirman, Rev. Mod. Phys. **73**, 357 (2001); D. Vion et al., Science **296**, 886 (2002).
- [4] A. Blais, A. M. van den Brink, and A. M. Zagoskin, Tunable coupling of superconducting qubits, cond-mat/0207112.
- [5] R. C. Ramos et al., IEEE Trans. On Appl. Supercond. to appear (2002).
- [6] A. J. Leggett, in Chance and Matter, edited by J. Souletie, J. Vannimenus, and R. Stora (Elsevier, Amsterdam, 1987), p. 395.
- [7] J. M. Martinis, M. H. Devoret, and J. Clarke, Phys. Rev. Lett. **55**, 1543 (1985); J. M. Martinis, M. H. Devoret, and J. Clarke, Phys. Rev. B **35**, 4682 (1987).
- [8] M. D. Feit, J. A. Fleck, Jr., and A. Steiger, J. Comput. Phys. **47**, 412 (1982); J. E. Bayfield, Quantum Evolution (John Wiley and Sons, Inc., 1999).
- [9] R. Yaris et al., Phys. Rev. A **18**, 1816 (1978); E. Caliceti, S. Graffi, and M. Maioli, Commun. Math. Phys. **75**, 51 (1980).